HELICOPTER DRAG MITIGATION DURING THE CARD PROJECT: NUMERICAL INVESTIGATION OF ROTOR-AND-PYLON FAIRINGS

D. Desvigne & D. Alfano
Airbus Helicopters S.A.S.
Marseille-Provence International Airport
F-13725 Marignane cedex
France

Abstract

A numerical analysis accompanying a wind-tunnel test campaign aimed at demonstrating benefits on drag of medium-weight multipurpose helicopter from advanced designs is presented in this paper. The work was performed within the frame of the CARD Partner Project (Contribution to Analysis of Rotor-hub Drag reduction), and was supported by the European Clean Sky JTI Green RotorCraft (GRC) Research Programme, which fosters the development of innovative technologies for more environmentally-friendly rotorcrafts.

The CARD wind-tunnel model is an accurate 1/4-scaled Airbus Helicopters H155 fuselage mock-up without rear parts. The model includes a 5-bladed rotor head. Two different innovative designs of pylon fairings, together with rotor fairings involving two enhanced sleeve fairings and two advanced hub-cap designs are considered.

Steady-state computations have been achieved using the unstructured-mesh based DLR's TAU solver to numerically assess the drag-reduction capabilities of around twenty different combinations of fairings. The ranking of combinations obtained from wind-tunnel drag measurements is well recovered numerically. The best combination provides an overall drag reduction by 9.7% of the baseline total drag. A comprehensive analysis reveals that the rotor/fuselage interactional effects, which account for 11% of the total drag of the baseline configuration, have been significantly mitigated in this case. The robustness of the benefits on drag obtained from the innovative fairings with respect to the angle of attack and sideslip angle is also presented.

In addition, numerical investigations have been carried out to assess the efficiency of the best combinations of the fairings designed within CARD for a complete helicopter, including the interactions with the rear parts, more realistic baseline sleeves, and additional spheriflex® rotor-head components such as the lead-lag dampers between the sleeves. The analysis shows that the benefits on drag are fairly well preserved for the best combinations in this more realistic context. Thus, CARD offers a promising contribution to potential full-scale application.

1. INTRODUCTION

Medium-weight twin-engine helicopters are versatile rotorcrafts representing in 2008 around 14% of the worldwide flight hours [16], and ensuring a very wide spectrum of missions: oil-and-gas transportation, law enforcement, search and rescue, emergency medical services as well as private and business transportation. Whatever potential global market evolutions in the next decades will be, such a wide application portfolio calls for a continuous challenge of rotorcraft operations environmental impact.

The Green Rotorcraft Integrated Technology Demonstrator (GRC ITD), as part of a wider Air Transport System considered in the Clean Sky Joint Technology Initiative (CS JTI), responds to this challenge, with the target of a more efficient usage of fuel in addition to a significant reduction of greenhouse gas emissions (up to 40% for CO_2, and 65% for NO_x) and noise radiation (10 EPNdB) throughout the whole mission range. In order to achieve those objectives, the GRC ITD promotes the development of new power plants, as well as advanced rotor blades and innovative technologies to reduce the power required to fly.

It has been recognized for decades that the rotorcraft aerodynamic drag is a first-order parameter which significantly impacts the required power [6][8][13][14]. As a consequence, special attention has been paid within the GRC ITD Project to mature innovative designs of airframe and non-lifting rotating components which offer reduced drag in cruise flight, together with a non-degradation of the overall lift and handling qualities.

The first phase of the GRC ITD Project consisted in a drag analysis of three different helicopter weight-classes. It was focused on discerning by CFD the rotorcraft components from which important benefits could be expected, depending on the specific architecture of each weight class. For the medium-weight class, which corresponds to helicopters of maximum take-off weight (MTOW) between 4 and 8 tons, Airbus Helicopters AS365 N3 & H155 B1 have been chosen as reference rotorcrafts. The main contributors to drag for

those references have been identified in [1] as the blade sleeves and the rotor-head/fuselage interactions, defined as the increase of the fuselage drag entailed by the presence of the rotor head. Whereas the parasite drag of the sleeves may be efficiently reduced with fairings [9][12][15], mitigating the rotor-head/fuselage interaction drag is much more challenging. Early investigations as described in [10][11], demonstrate that the hub-cap design, as well as the shape of the pylon fairing, are amongst key elements to reduce the interaction drag. Indeed, pylon fairings are usually the place of important interactions with the wake generated by the rotor head, this wake being also highly affected by the downwash created by the lifting hub cap [1][11].

This is why Airbus Helicopters' innovative designs of pylon fairings, as well as rotor fairings involving enhanced sleeve fairings and advanced hub-cap designs were proposed to be experimentally investigated within the framework of the Clean Sky CARD Consortium (Contribution to Analysis of Rotor-hub Drag reduction), composed of the Aircraft Research Association (ARA), University of Glasgow, Výzkumný a Zkušební Letecký Ústav (VZLÚ), with Airbus Helicopters as topic leader. Further numerical studies were performed at Airbus Helicopters.

The main objective was to rank the different combinations of fairings in order to identify the most efficient combination in terms of drag mitigation together with a non-degradation of the lift.

2. BACK TO THE 'CARD' WTT CAMPAIGN

The Wind-Tunnel Tests (WTT) were conducted in the 3m diameter low-speed wind tunnel at VZLÚ in Prague (Czech Republic). A comprehensive description of the experimental set-up & methodology, as well as a data analysis, has already been reported in [4].

Additional elements are presented in this section, for further comparisons with numerical results.

2.1 Model description

The CARD Wind-Tunnel model is an accurate 1:4 scale Airbus Helicopters H155 fuselage. Engine intakes are plugged. The Fenestron® and tail parts are not implemented, but the tail-boom includes the Fenestron® shaft tunnel. The tail-boom ends with an aerodynamically smooth stopper, and there are no panel seams or any other surface excrescences.

The model is mounted by a 5-bladed rotor head tilted forwards by 4°, and composed of a mast, a hub, a hub cap, sleeves, blade roots, and truncated rigid blades for which a third of the original blade span has been retained, as illustrated in Figure 1. This presents the advantage that the complexity of the full rotor-system aeromechanics has been drastically reduced, but the interaction effects in the blade hub region are preserved. It also includes non-functioning control rods. The rotor-hub design allows the blade collective pitch angle to be set to discrete angles; it has been fixed to 8° for all the results presented in what follows. The blade roots were fixed to blade sleeves attached to the rotor mast. Blade sleeves form a realistic but rigid aerodynamic representation of the blade mounting flexures on the H155. Aerodynamic representation of the lead-lag dampers was not included in the rotor-hub design.

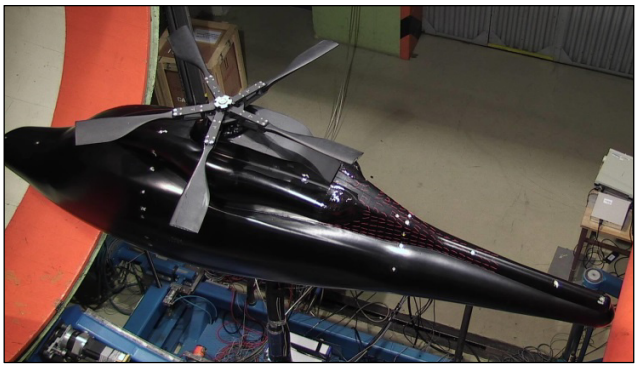

Figure 1 – Overview of the 1:4 scale Airbus Helicopters H155 CARD model (without hub cap) in the VZLÚ wind tunnel

2.1.1 Pylon fairings

Three different designs based on description of [1] of the aft portion of the pylon fairing were fitted to the model. They are shown in Figure 2. The H155 baseline pylon fairing is referred to as F0. Advanced concepts F1 and F2 are constructed from the dimensional characteristics of the baseline design. They principally differ from it by the implementation of a trailing bump at the back panel. Both shapes ensure at the aft portion of the pylon fairing the same vertical-bending angle. The lateral-lip terminations of the baseline shape have been redesigned in depth, and lips were extended to the pylon-fairing's trailing panel for F1 and F2 concepts. The F1 shape offers lateral ripples both on the sides and the trailing panel of the pylon fairing, while the F2 concept exhibits flat sides and ripples are only implemented at its trailing panel. The concept F2 has been numerically tested only.

2.1.2 Blade-sleeve fairings

Two different sets of blade-sleeve fairings were considered. Partial fairings S1 cover the upper and lower flanges of the baseline blade-sleeve design, while full fairings S2 cover the entire sleeve. Both advanced fairing concepts present an improved cross-sectional profile to the flow and were designed for improved drag performance. An overview of the different sleeve fairings is proposed in Figure 2. The fairing capabilities of the CARD concepts S1 and S2 are illustrated in Figure 3.

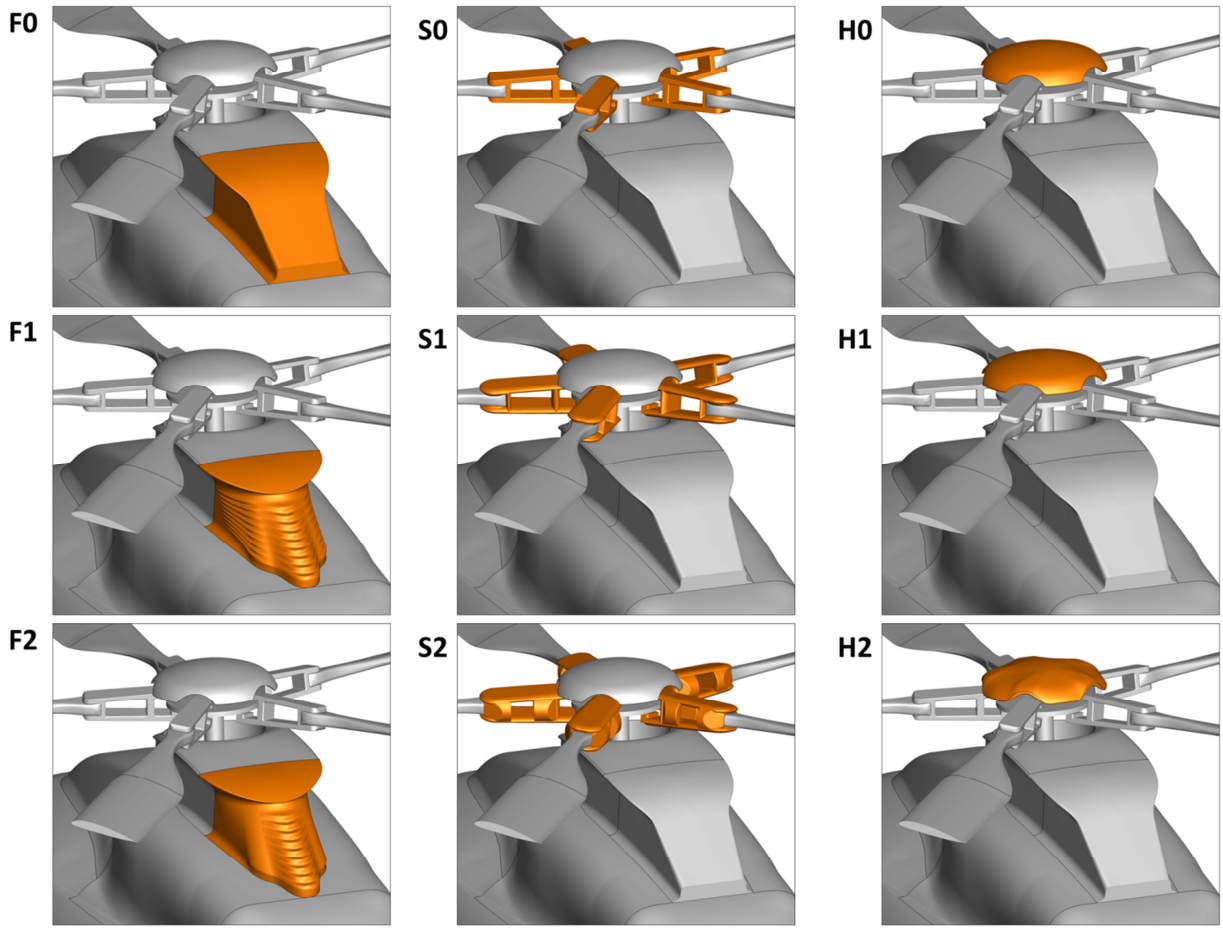

Figure 2 – Overview all the shapes investigated within the CARD project; Pylon fairings, sleeve fairings, and hub caps are rspectively referred to as F*n*, S*n*, H*n*, and are highlighted in orange; n = 0 stands for H155 baseline shape, *n* = 1 and *n* = 2 represent respectively the first and the second variation of the advanced CARD concepts

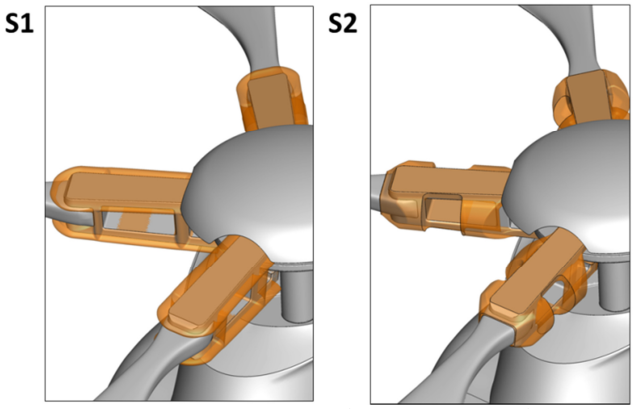

Figure 3 – Fairing capabilities of the CARD sleeve-fairing concepts S1 and S2

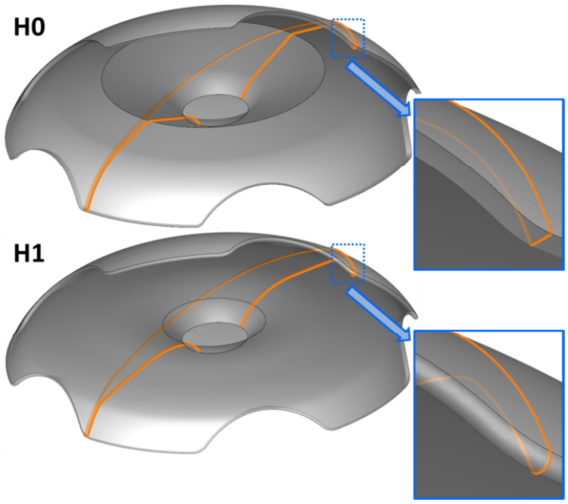

Figure 4 – Sketch of the CARD hub-cap profiles for H0 & H1

2.1.3 Hub caps

Three different hub caps were fitted to the rotor. The baseline hub cap was an accurate, scale model of the H155 beanie. One modification of the hub cap is designed with rounded corners at the hub-cap edges and is constructed from a thicker profile (H1). The second concept is an innovative design characterized by five azimuthal waves at the upper surface profile and by rounded edges (H2), as described in [2]. Sketches of the hub-cap profiles are proposed in Figure 4.

2.2 Load cells

The model has been designed to ensure measurements of the rotor system forces and fuselage forces separately. Thus, the fuselage was attached onto the live side of the VZLÚ strut balance, while the rotor system was attached to the ground side of the strut balance. Two co-axially load cells, coincident with the rotor axis and rotating with the rotor shaft, were used to support the rotor and hub cap independently. The VZLÚ strut balance and the two rotating load cells all measured all three orthogonal forces and moments. The methodology for extracting drag surfaces is exposed in details in [4].

2.3 Flow conditions

Flight conditions considered for the drag reduction assessment correspond to cruise conditions. Down-scaling of the full-scale cruise conditions is achieved by considering a constant advance ratio of 0.365. All the parameter values are summarized in Table 1. Angles of attacks between -8° and 0° have been considered in order to fully cover the scope of possible combinations of weight and balance.

VARIABLE	UNIT	FULL SCALE	WTT SCALE
Scale	[—]	1	0.25
Rotor radius	[m]	6.30	1.575
Rotor diameter	[m]	12.60	3.15
Rotorcraft velocity	[kt]	160	87.5
Rotorcraft velocity	[m/s]	82.3	45.0
Rotor velocity	[rpm]	342	748
Advancing ratio	[—]	0.365	0.365
Blade-tip Mach number (adv.)	[m/s]	0.889	0.486
Reynolds Ratio Full Scale/WT	[—]	—	7.31

Table 1 – Downscaling of the full-scale cruise conditions

2.4 Results

2.4.1 Non-spinning vs. spinning rotor head

The effect of the rotation of the rotor on the total drag is evaluated in this section. The general trend presented in what follows has been verified for several configurations, and it is presented for the combinations F0S0H0 and F0S1H0. When the rotor head is non-spinning, two azimuthal locations are proposed, namely 0° and 36°, corresponding to the presence of a front blade or a back blade respectively, as shown in Figure 5. Drag surfaces have been normalized by the drag measured for the case of a spinning rotor head and for an angle of attack of 0°.

Figure 6 shows the drag surface CdS measured with respect to the angle of attack within the range [-8°, 0°], for a null sideslip angle. The drag polars obtained in the case of a rotating rotor head and for the non-spinning one exhibiting a front blade (0° of azimuth) are in good agreement, both in terms of overall dynamic drag (dCdS/dα), but also in terms of drag magnitude. In the case of a non-spinning rotor head located at azimuth 0°, the drag increases by 1% to 6% of the total average drag measured for the F0S0H0 configuration with a spinning rotor. For F0S1H0, a discrepancy up to 2% is experienced over the polar.

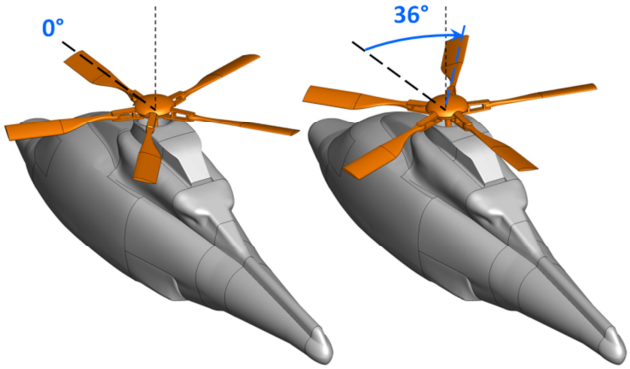

Figure 5 – Azimuthal locations investigated for configurations with a non-spinning rotor head; left: 0° (front blade); right: 36° (back blade)

For the case of a non-spinning rotor head with a back blade (36° of azimuth), the variation of drag with the angle of attack is much more flat, and discrepancies with the drag surface measured for the configuration with a rotating rotor head are important, especially for large negative angles of attack.

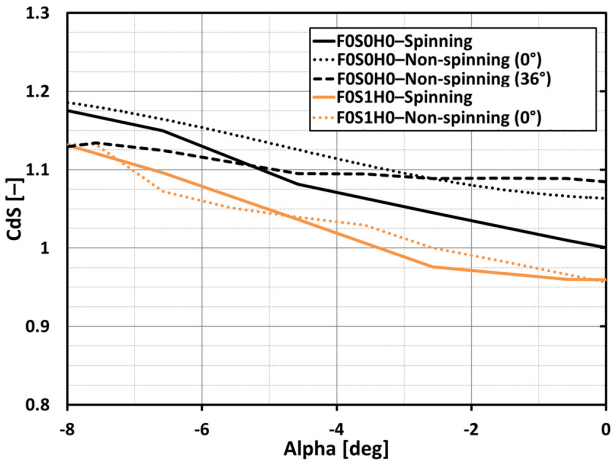

Figure 6 – Drag polar for the baseline configuration F0S0H0 (in black), and combination F0S1H0 (in orange), with a non-spinning rotor head at azimuth 0°, 36° or with a spinning rotor head; incoming flow velocity of 45 m/s, 0° of sideslip angle; Drag surfaces CdS are normalized by the drag of F0S0H0 measured in the case of a spinning rotor head for angle of attack of 0°

Thus, those comparisons tends to indicate that non-rotating frames can be considered for drag assessment for the numerical campaign, provided the rotor head has a fixed azimuthal location of 0°. This result significantly reduces the complexity of the numerical campaign, as steady-state simulations may be deployed to evaluate the drag of multiple combinations instead of time-consuming simulations involving a spinning rotor head.

Nevertheless, in order to fulfil the GRC ITD Project objectives, the non-degradation of lift also has to be assessed. This has been investigated during the CARD WTT, and unsurprisingly, the experimental analysis demonstrates that a spinning rotor must be considered to obtain reliable evaluations of the lift generated by the model, as illustrated in Figure 7. Accordingly, lift is not investigated numerically in what follows, because a non-spinning rotor was implemented in the simulations (see Section 3).

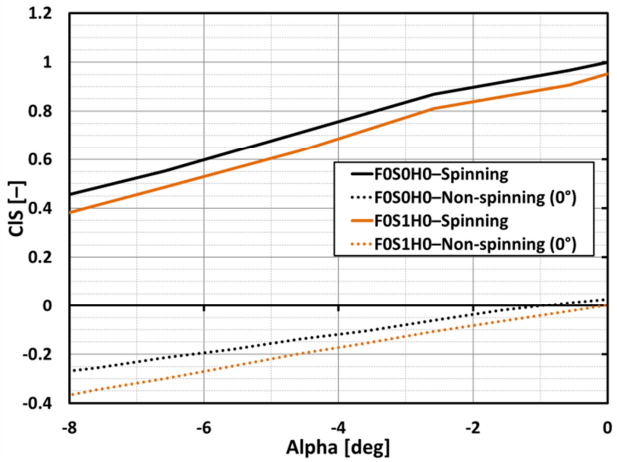

Figure 7 – Lift polar for the baseline configuration F0S0H0 & F0S1H0, with a non-spinning rotor head at azimuth 0° or with a spinning rotor head; incoming flow velocity of 45 m/s, 0° of sideslip angle; Lift surface ClS are normalized by the lift of F0S0H0 measured in the case of a spinning rotor head for angle of attack of 0°

2.4.2 Global benefits on drag for 0° angle of attack

Figure 8 shows the total drag surface CdS measured for an angle of attack of 0° for each configuration accounting for a spinning rotor. Drag surfaces have been normalized by the total drag surface of the baseline combination F0S0H0. It reveals that:

- The best combination is the baseline pylon fairing together with the partial sleeve fairings S1 and the smooth hub cap H1. This combination ensures benefits on drag of 6.6% of the total drag measured for the baseline configuration with a targeted angle of attack of 0°. The same combination for which the hub cap has been replaced by the pulsating hub cap H2 is also a very good candidate for significant drag reduction (–6.0%);
- Pylon fairing F1 always entails more drag than the baseline pylon fairing F0 for a given combination of sleeve fairings and hub caps;
- Partial sleeve fairings S1 always ensure larger benefits on drag than full fairings S2 for a given combination of pylon fairings and hub caps;

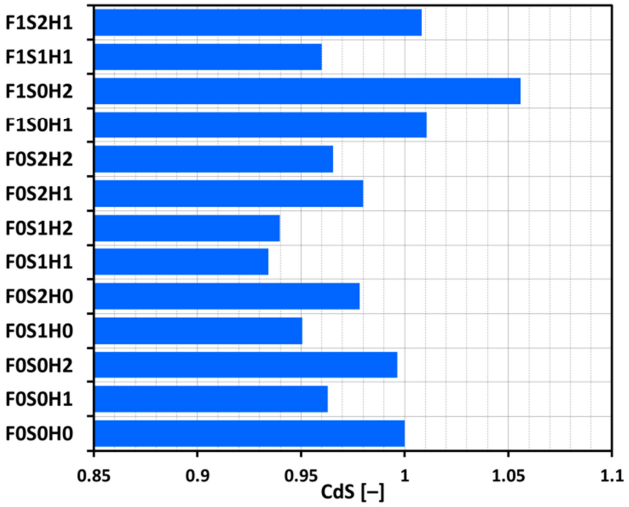

Figure 8 – Total drag surface CdS for each configuration, normalized by the drag surface of the baseline configuration F0S0H0; angle of attack of 0°; spinning rotor

- Hub cap designs H1 and H2 are always more efficient than baseline hub cap H0 for drag reduction objective;
- The benefits on drag from the use of rotor-head fairing S1H1 is smaller than the sum of the benefits on drag coming from the use of partial sleeve fairing S1 only (F0S1H0), and from the use of the smooth hub cap (H1) only (F0S0H1);
- The benefits on drag from the use of combination S1H2 is greater than the sum of the benefits on drag from the use of partial sleeve fairing only (F0S1H0), and from the use of the pulsating hub cap (H2) only (F0S0H2).

Because loads have been measured separately at the hub cap, rotor, and fuselage, it is possible to assess the contribution of the parasite drag reduction and interactional drag reduction to the overall benefits on drag. This is what is presented in Figure 9. It is observed that:

- For the baseline configuration F0S0H0, the rotor is responsible for 43% of the total model drag. The hub cap contribution is 9% and the fuselage drag is 48% of the total drag;
- For the combination F0S1H1, around 50% of the benefits on total drag come from a reduction of the interactional drag at the fuselage which is significant. The other 50% come from a reduction of the rotor-head parasite drag with the innovative fairings.

2.4.3 Robustness of the benefits on drag

The variations of the model drag surface with respect to the angle of attack are presented in Figure 10, for each combination of fairings.

It shows that for the best combination F0S1H1, the benefits on drag are very well preserved within the range [-8°;0°]. This is also true for the combination F0S1H2 which is

another good candidate offering important drag mitigation all over the range of investigation. Combinations involving the innovative pylon fairing F1 exhibit a less regular drag polar, compared to what measured when the baseline pylon fairing is used, especially in the range of angles of attack [-4°;0°].

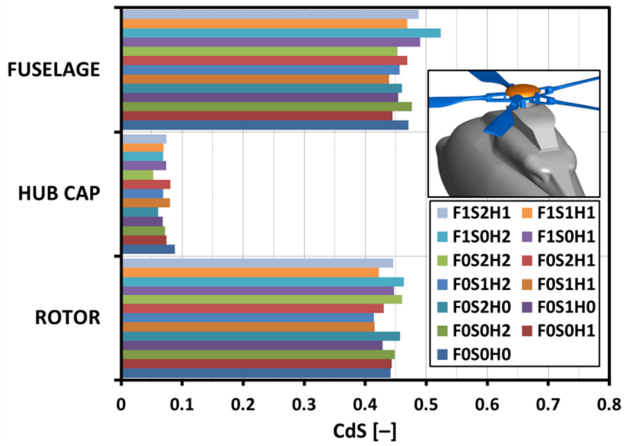

Figure 9 – Drag distribution for each configuration, normalized by the drag of the baseline configuration F0S0H0; angle of attack of 0°, spinning rotor

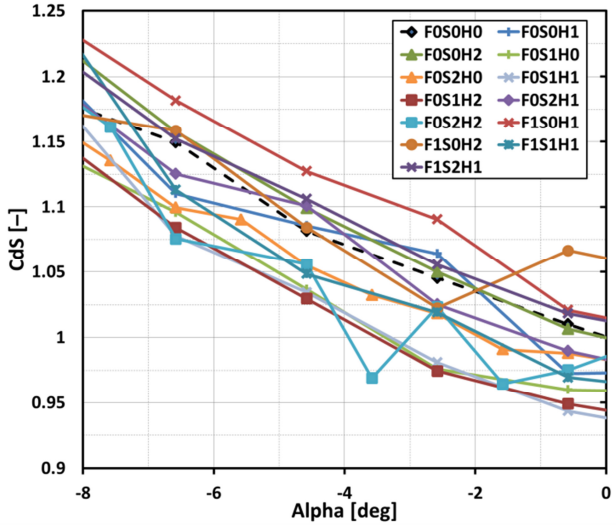

Figure 10 – Drag polar for each configuration (with a spinning rotor), normalized by the drag surface of the baseline configuration F0S0H0 for an angle of attack of 0°

2.4.4 Non-degradation of lift

In this section, the impact on lift of different combinations of fairings is investigated. Figure 11 shows lift polar for some configurations. It reveals that the lift generated by the best combination in terms of drag (F0S1H1) is fairly well preserved with respect to the baseline over the range [-6°,0°]. The configuration F0S2H1 is also demonstrated to always generate more lift than the baseline over the range of investigation. It means that the rotor power may be slightly reduced to ensure the baseline overall lift, which leads to an indirect reduction of the rotor drag, to be added to the 2% of benefits on drag presented in Figure 8.

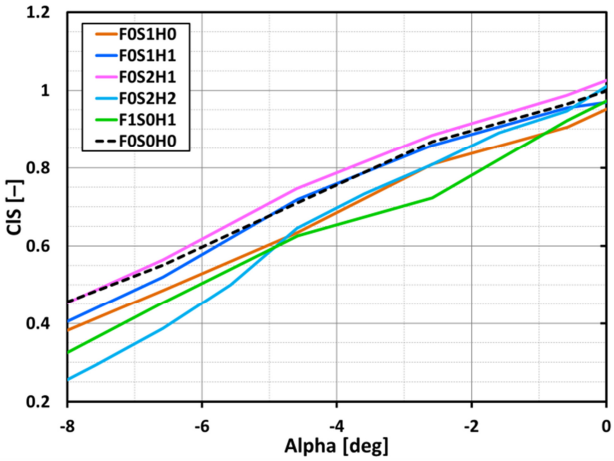

Figure 11 – Lift polar for some configurations (with a spinning rotor), normalized by the lift surface of the baseline configuration F0S0H0 for an angle of attack of 0°

In what follows, the ranking of combinations of fairings with respect to drag, as well as the robustness of corresponding benefits is investigated numerically. The concept F2 is included in the numerical analysis.

3. COMPUTATIONAL PROCEDURE

Estimating numerically drag forces over bodies demands accurate simulations of the flow developing around them, which remains quite challenging for a fuselage-mounted rotor hub of a helicopter [8]. The global flow is usually the result of numerous interactions between all the rotor-hub subcomponents and the fuselage. Accordingly, investigating the aerodynamic characteristics of each rotor-head subcomponent separately is usually irrelevant for a global understanding of rotor-head flows, because their isolated aerodynamic behavior is severely altered when they operate together with all other rotor-hub subcomponents and the fuselage's upper deck [8]. Another difficulty comes from the very complex geometry of the rotor head, exhibiting numerous details, sharp angles, and cavities.

3.1 Description of the numerical model

The shapes investigated numerically are high-fidelity representations of the WT model as represented in Figure 2. The rotor head is not spinning for all the computations. The use of a fixed rotor head azimuthally located at 0° is motivated by the experimental results presented in section 2.4.1.

In order to assess the drag generated by each subcomponent, the numerical model has been split into 13 different families, as illustrated in Figure 12. In particular, a family is dedicated to the aft pylon fairing and another to the aft cowlings, in order to assess the interactional drag

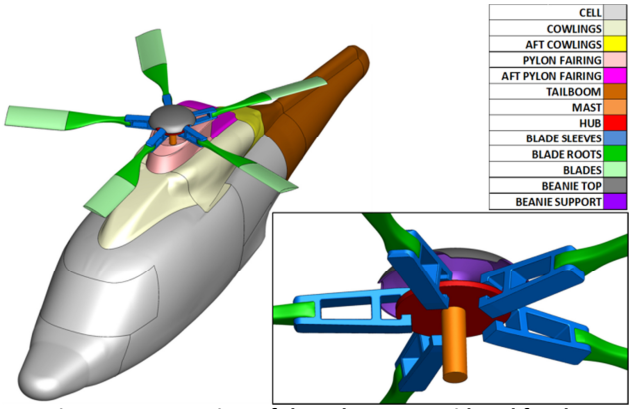

Figure 12 – Overview of the subparts considered for the numerical investigations

PARAMETER	VALUE
Equations solved	Reynolds Averaged Navier-Stokes
Solver	DLR's TAU
Solver's version	2013.1.0
Turbulence model	k–ω with SST Menter correction
Spatial schemes	Viscous fluxes: 2nd order central scheme with artificial scalar dissipation; Turbulent fluxes: Roe's scheme with 2nd order least-square gradient reconstruction
Fictive time stepping	2nd order backward Euler
Multigrid	Yes, 1-order V-cycle
CFL number	2
Residual of density	Reduction by 4 decades

Table 2 – Solver methods & parameters

mitigation for those components, usually propitious to interactional drag generation.

3.2 CFD solver and numerical features

All the geometries presented in this work have been meshed using ICEM CFD at wind-tunnel scale (1:4). It consists in a non-structured mesh based on roughly 150 million of elements for the configurations without the rotor head, and up to 180 million of elements for the most complex models. 24 layers of prisms have been required to mesh properly boundary layers at the fuselage and at the rotor-head's elements, ensuring a mean dimensionless wall distance y^+ of roughly 1. The prism-layers are grown by resorting to a bottom-up based method. Two boxes of mesh refinement have been required at the vicinity of the fuselage and in the vicinity of the rotor-head parts, in order to capture the wake generation and airframe/wake interactions. For all the configurations, a mesh quality greater than 0.05 has always been ensured. Mesh quality is evaluated from elements' aspect ratio.

The steady-state Navier-Stokes equations (RANS) have been solved numerically using DLR's TAU 2013.1.0 code [17] with all the numerical methods and parameters reported in Table 2. Overviews of meshes are proposed in Figure 13.

3.3 Flight conditions

The same flight conditions as the ones considered during the WTT campaign (Table 1) have been used for the numerical simulations, assuming sea-level altitude and ISA atmospheric conditions. A collective pitch angle of 8° has been considered for those flight conditions.

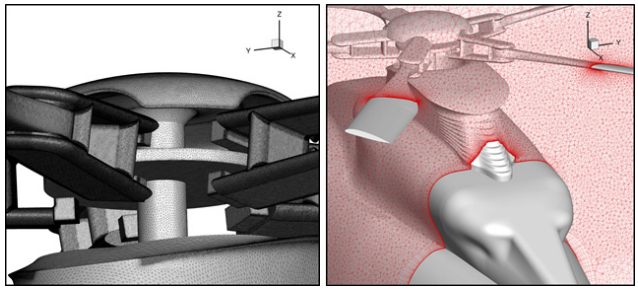

Figure 13 – Overview of the skin and volume meshes (F1S1H1)

4. NUMERICAL RESULTS

4.1. Convergence

A total of 60,000 iterations have been required for each run in order to ensure a reduction of 4 to 5 decades for the total residual of density, as illustrated in Figure 14.

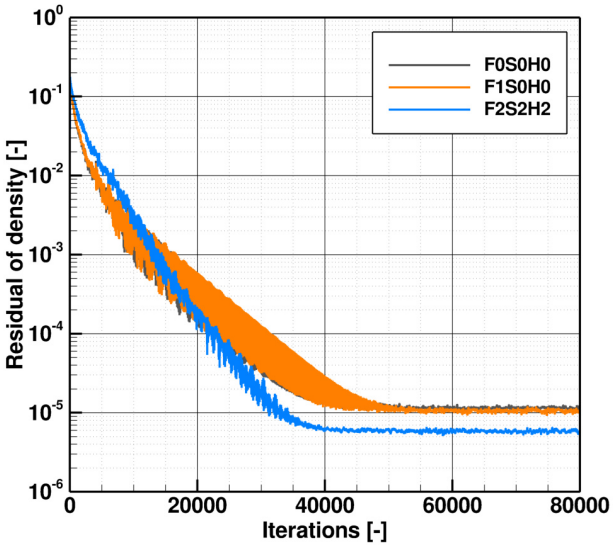

Figure 14 – Examples of history of the total residual of density; the total residual has been normalized by its initial value; angle of attack of 0°

The history of the drag surface of some subcomponents is exhibited in Figure 15. Almost constant loads are experienced, pointing out the fair convergence level of the steady-state computations. Some components, such as aft cowlings, show slight oscillations in the flat zone, because of the natural unsteadiness of the flow around them or strong interactions with the rotor-head's wake. Mean drag surfaces have been estimated by averaging instantaneous data over

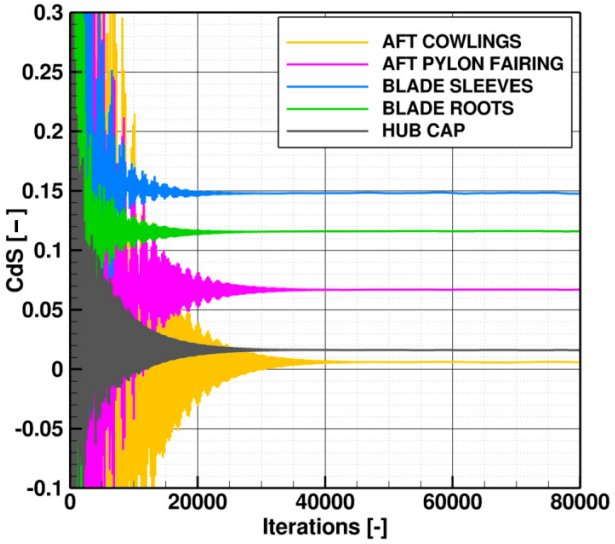

Figure 15 – Example of history of the dimensionless drag surface for some F0S0H0's subcomponents; drag surfaces have been normalized by the model total drag; angle of attack of 0°

additional 20,000 iterations in order to get rid of those oscillations.

4.2. Some comparisons with WTT measurements

Extensive comparisons have been carried out during the CARD project. A sample is presented in what follows. Figure 16 shows for different combinations of fairings a comparison of the drag polar obtained numerically with a fixed rotor with the polar measured during the WTT campaign, accounting for a spinning rotor.

For all the combinations, the experimental polars are underestimated by CFD by 4 to 10% all over the range of considered angles of attack, the discrepancies being roughly constant. As reported in Figure 6, the discrepancies would have been slightly larger if experimental polars accounting for non-spinning rotor had been considered. This is not a big issue, as the main goal is to rank the different combinations together with an evaluation of the drag benefits in proportion to the baseline drag level. The discrepancies are suspected to principally come from the use of dissipative 2nd-order numerical schemes in the simulations. Nevertheless, numerical & experimental polars are in good agreement in terms of magnitude of the variations of drag with respect to the angle of attack. In addition, the ranking of combinations regarding the benefits on drag is well predicted by CFD. Accordingly, despite the underestimation of the drag levels, the use of CFD is fairly reliable to assess the robustness in terms of benefits on drag over the whole range of considered angles of attack, as well as to rank the combinations of fairings regarding the drag-reduction capabilities.

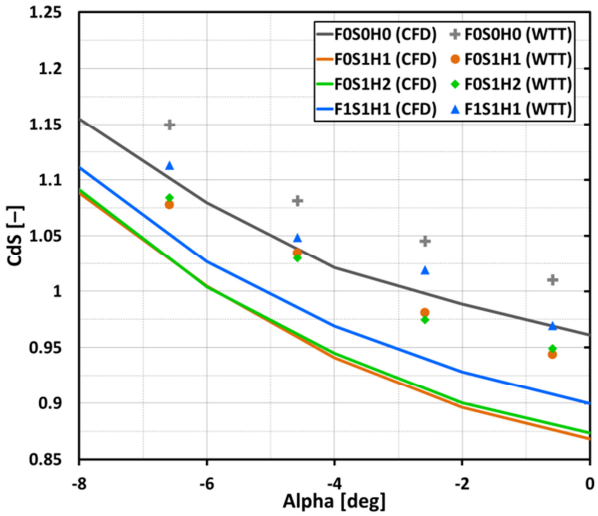

Figure 16 – Drag polars for some combinations of fairings obtained experimentally for a rotating rotor (WTT) and numerically with a fixed rotor (CFD); Drag surfaces are normalized by the total drag obtained experimentally for the baseline configuration (F0S0H0); angle of attack of 0°

4.3. Benefits on drag

4.3.1 Global benefits for an angle of attack of 0°

Figure 17 summarizes the parasite drag, the interactional drag and the total drag surfaces for all the different combinations for an angle of attack of 0°. For the sake of consistency, drag surfaces have been normalized by the total model drag of the baseline configuration obtained numerically. It reveals that:

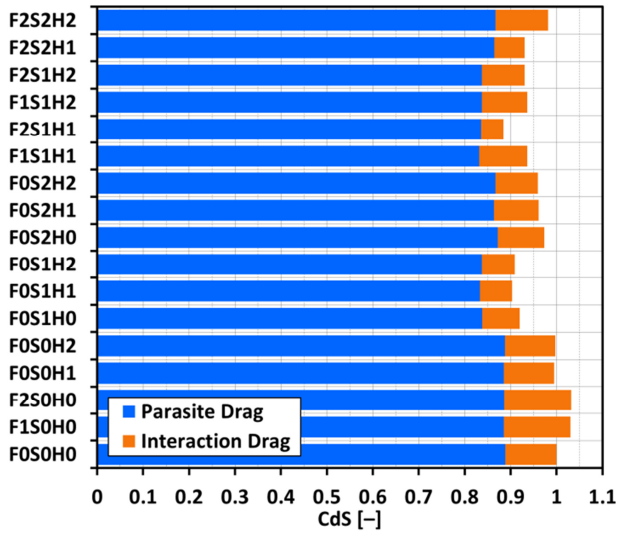

Figure 17 – Total drag surfaces as a function of the combinations of fairings; parasite drag in blue, interactional drag produced at the fuselage in orange; Drag surfaces are normalized by the total model drag of the baseline configuration obtained numerically; angle of attack of 0°

- For the baseline configuration, the interactional drag accounts for 11% of the total model drag;
- Amongst the combinations of fairings tested during the WTT campaign, the best combination is the baseline pylon fairing F0 together with the partial sleeve fairings S1 and the smooth hub cap H1, as ranked during WTT. This combination ensures benefits on drag of 9.7% of the numerical model total drag. The same combination for which the hub cap has been replaced by the pulsating hub cap H2 is also a very good candidate (–9.1% of the model total drag). Those benefits — expressed in % of the baseline configuration — are slightly greater than what measured during the WTT campaign because the reference drag is numerically smaller than the experimental reference (cf. Figure 16);
- The overall best combination of rotor-head fairing is S1H1, together with the innovative pylon fairing F2. The benefits on drag reach up to 11.6% in this case, but it cannot be compared with WTT results;
- Pylon fairing F1 entails more drag than the baseline pylon fairing F0, for a given combination of sleeve fairing and hub cap design, which is also what observed in the WTT. Innovative pylon fairing F2 is a source of additional drag reduction when it is used with some specific combinations of rotor-head fairings;
- Partial sleeve fairings S1 ensure larger benefits on drag than when sleeve full fairings S2 are used, for a given combination of pylon fairing and hub cap design;
- Hub cap designs H1 and H2 are always more efficient in terms of drag reduction than the baseline hub cap H0.

4.3.2 Drag distribution for an angle of attack of 0°

A global drag distribution is presented in Figure 18 for each configuration, for an angle of attack of 0°. It is shown that:

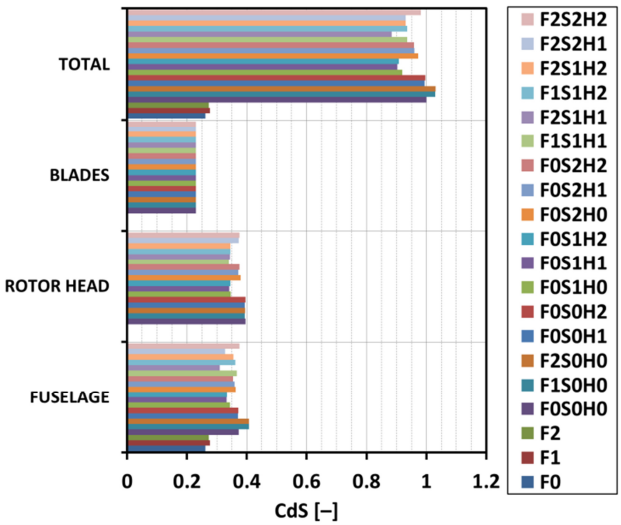

Figure 18 – Drag distribution as a function of the combinations of fairings; Drag surfaces are normalized by the total model drag of the baseline configuration obtained numerically; angle of attack of 0°

- The rotor-head fairing S1H1 ensures the best reduction of the rotor parasite drag, by roughly 5% of the total drag of the baseline configuration, hence representing respectively 55% and 40% of the total benefits when it is used with pylon fairing F0 and F2;
- Both innovative pylon fairings F1 and F2 are responsible for an increase of the total model drag, except when they are used together with some specific combinations of sleeve fairings and hub cap designs;
- The interaction drag (at fuselage) is significantly reduced when combinations S1H1 or S1H2 are used. When the innovative pylon fairing F2 if fitted to the upper deck, the rotor combination S1H1 is more efficient in terms of drag reduction than combination S1H2. This is the result of different hub-cap/fuselage interactions in this particular case;
- The reduction of the interactional drag at the fuselage contributes to 4.5% of the total drag of the baseline configuration for F0S1H1 (i.e. 45% of the total benefits), and up to 7.3% for F2S1H1, thus representing up to 70% of the total benefits.

4.3.3 Reduction of rotor/fuselage interactions

As rotor/fuselage interactions contribute to 40% to 70% of the benefits on drag for the best combinations of fairings, it is relevant to analyse how the wake generation has been modified by the innovative CARD fairings. Obviously, only full unsteady CFD simulations may provide reliable data concerning wakes. Nevertheless, some rough information may be extracted from a volume-data analysis of less demanding steady-state simulations.

Figure 19 & Figure 20 show a map of dynamic pressure deficit in two transversal planes, located respectively behind the rotor head and pylon fairing, for two combinations of fairings, namely the baseline one (F0S0H0) and F2S1H2. The dynamic pressure deficit $\Delta q\ (\%)$ is evaluated as:

$$\Delta q(\%) = 100\frac{q - q_\infty}{q_\infty} = 100\left(\frac{\rho\|\boldsymbol{U}\|^2}{\rho_\infty\|\boldsymbol{U}_\infty\|^2} - 1\right)$$

where ρ is the local density of the fluid, and $\boldsymbol{U}$ the local mean velocity vector. The subscript ∞ stands for far-field data.

Reducing the drag of the hub and pylon generally reduces the wake generation and dynamic pressure deficit downstream [7]. As a consequence, the quantity Δq may be used as a global indicator for wake visualization purpose. Of course, other indicators could have been used, such as longitudinal vorticity or the Q-criterion [5].

Figure 19 demonstrates that areas of strong dynamic pressure losses have been reduced by the use of sleeves fairings S1 in combination with the pulsating hub cap H2. Figure 20 shows that the rotor-head fairings reduce the magnitude of dynamic pressure deficit at the vicinity of the pylon fairing. This tends to demonstrate a mitigation of rotor-head/pylon interactions, which contributes to a reduction of the interactional drag accordingly.

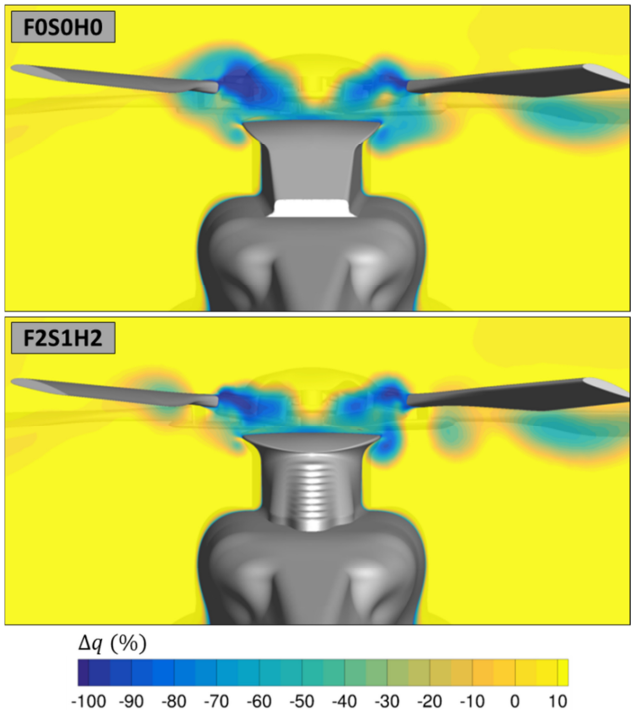

Figure 19 – Dynamic pressure deficit in a transversal plane behind rotor head, normalized by farfield dynamic pressure; angle of attack of 0°

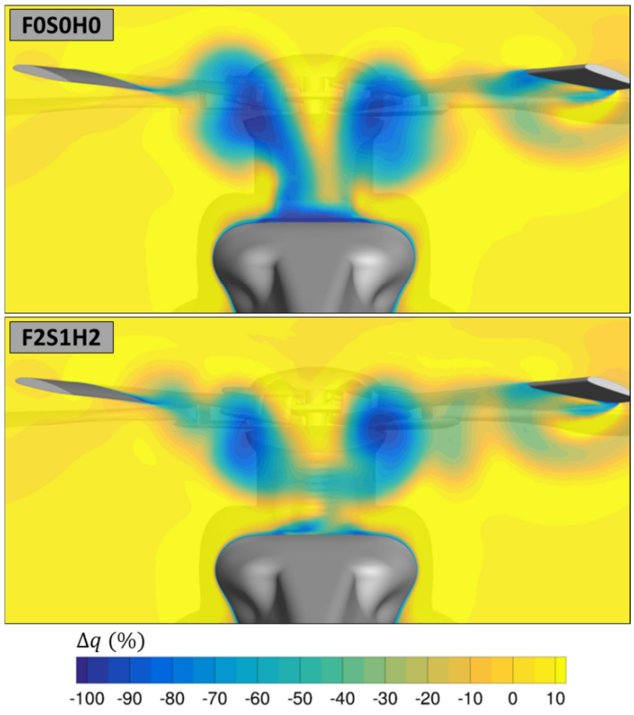

Figure 20 – Dynamic pressure deficit in a transversal plane behind the aft portion of pylon fairing, normalized by farfield dynamic pressure; angle of attack of 0°

4.4 Robustness of the benefits

The robustness of the benefits on drag is an important aspect for full-scale applications; depending on the mass & balance as well as the weather conditions, the angle of attack and sideslip angles may be fairly different from (0°, 0°), as considered in section 4.3.

4.4.1. Angles of attack

The variations of the total model drag surface with respect to the angle of attack are presented in Figure 21, for each configuration. It shows that the benefits on drag are very robust over the range [-8°, 0°] for the best combinations as identified during the WTT campaign (F0S1H1 and F0S1H2), but also for the combination F2S1H1. It also shows that the ranking of the different combinations established for an angle of attack of 0° in the previous section is very well preserved for the other angles of attack investigated in this work.

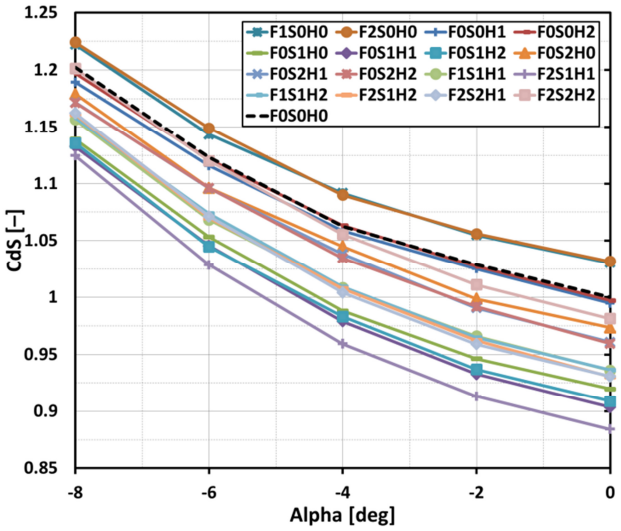

Figure 21 – Drag polar with respect to the angle of attack, for each combination of fairings; Drag surfaces are normalized by the total model drag of the baseline configuration; sideslip angle of 0°

4.4.2. Sideslip angles

The variations of the total model drag surface with respect to the sideslip angle are shown in Figure 22, for the baseline configuration and for some combinations of fairings. The good robustness of the benefits on drag is demonstrated for a wide range of sideslip angle, from -10° to 0°.

5. CARD SHAPES ON A COMPLETE HELICOPTER

In this section, the drag reduction capabilities of the best CARD combinations are investigated for the highly complex and more realistic shapes of the rotor head, accounting for the lead-lag dampers.

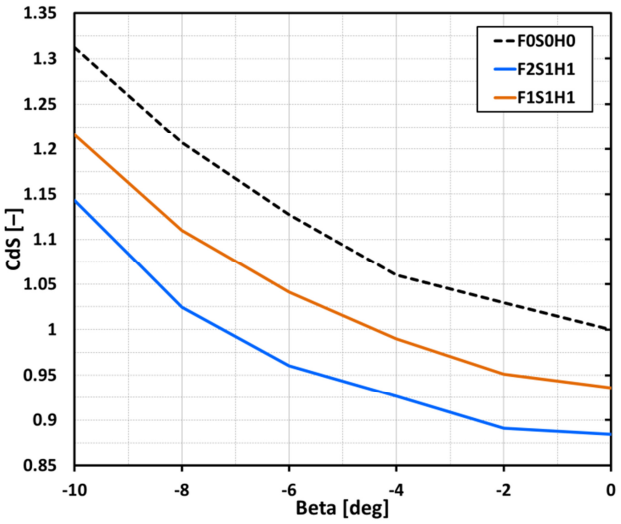

Figure 22 – Drag polar with respect to sideslip angle, for each combination of fairings; Drag surfaces are normalized by the total model drag of the baseline configuration; angle of attack of 0°

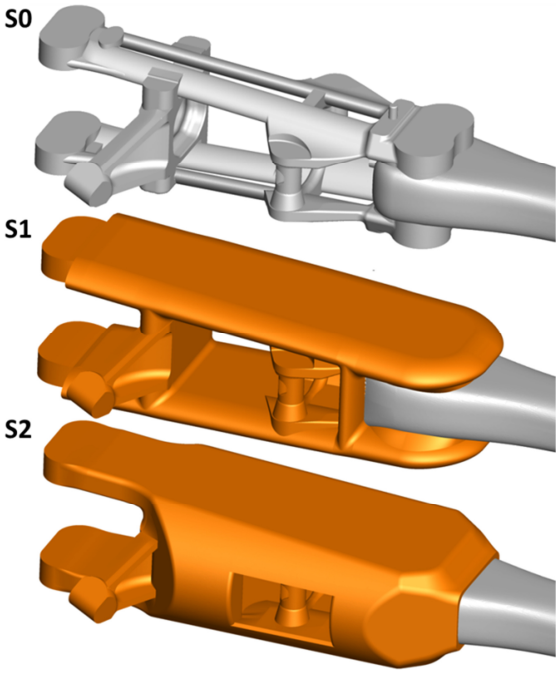

Figure 23 – Overview of the CARD sleeve fairings adapted to the high-fidelity shape of the baseline sleeve, including junctions to the lead-lag dampers and to the control rods

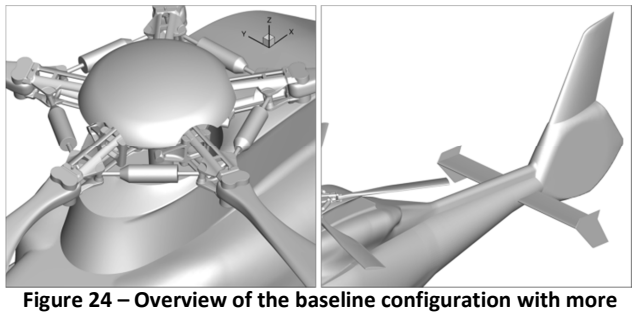

Figure 24 – Overview of the baseline configuration with more realistic rotor head (left), and rear parts (right)

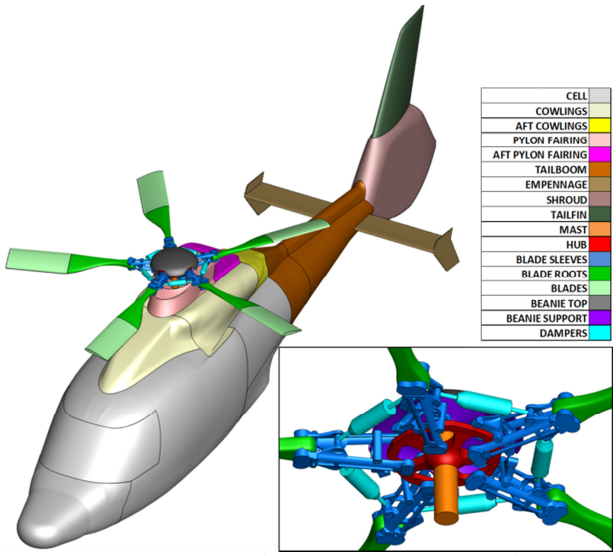

Figure 25 – Overview of the subparts considered for the complete-helicopter investigations

5.1 High-fidelity geometries

The CARD innovative fairings have been adapted to the more realistic shape of the baseline sleeves, as shown in Figure 23. The tail parts have also been taken into account in the numerical model, so that the potential interactional drag at the rear parts is considered, as shown in Figure 24.

The Fenestron®'s shroud has been plugged in this study, and the rotor is not represented accordingly. Only F0, F1, F2, F0S0H0 and F2S1H1 combinations are considered. Because the presence of the dampers may partially jeopardize the benefits on drag from the use of partial sleeve fairings, the additional combination involving full sleeve fairings F2S2H1 has also been considered. In order to assess the drag generated by each subcomponent, the numerical model has been split into 16 different families, as illustrated in Figure 25.

5.2 Numerical features

Meshes have been constructed based on the same methodology as described in section 3.2. Because of the inclusion of much more details at the rotor head and tail parts, around 250 million of elements have been required for the most-demanding mesh. Flight conditions considered in

this section correspond to conditions described in Table 1. Numerical parameters of the simulations are summarized in Table 2.

5.3 Results

5.3.1 Benefits on drag for an angle of attack of 0°

Figure 29 shows the total drag surfaces for an angle of attack of 0°, as a function of the different combinations. Both parasite drag and interactional drag are represented. It reveals that F2S1H1 and F2S2H1 ensure benefits on drag of around 6.5% of the total baseline drag. The parasite drag appears to be only slightly reduced at the rotor head, and the benefits mostly come from a reduction of the interactional drag generated at the upper deck and tail parts. Interactional drag accounts for roughly 12% of the total drag of the baseline configuration.

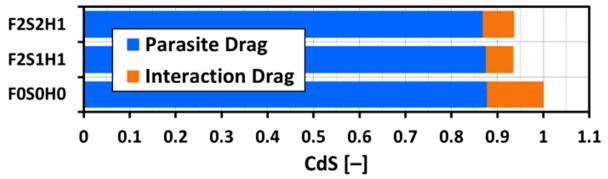

Figure 26 – Total drag surfaces as a function of the combinations of fairings; parasite drag in blue, interactional drag produced at the fuselage in orange; Drag surfaces are normalized by the total model drag of the baseline configuration obtained numerically; angle of attack of 0°

The modifications of the generation of pressure drag by the CARD fairings may be locally investigated at the fuselage. Comparisons of the skin-distribution of coefficient of pressure at the aft upper deck between the baseline F0, the isolated fuselage F2 on the one hand, and configurations with a rotor F0S0H0 & F2S1H1 on the other hand are proposed in Figure 27.

It highlights that positive coefficient of pressure is recovered at the aft portion of the isolated innovative pylon fairing F2. This positive coefficient of pressure consequently tends to create a pushing effect, given the shape of the aft chimney, which is beneficial to mitigate the total model drag. The phenomenon is a bit exacerbated by the presence of the rotor-head fairing S1H1. In addition, coefficient of pressure at aft cowlings is shown to slightly increase when S1H1 is used in conjunction with pylon fairing F2.

Drag at tail parts is also impacted by the CARD innovative fairings. A direct comparison of the coefficient of pressure at the tail-part skin reveals that the coefficient of pressure has been reduced at the base of shroud close to the junction with tail-boom, as illustrated by Figure 28.

5.3.2 Robustness of the benefits

In order to assess the robustness of the best combinations of fairings, the total drag polar has been considered for angles of attack within the range [-8°;0°], as illustrated in Figure 29. The benefits on drag appear to be fairly well preserved for the investigated range; indeed a constant drag reduction representing 5% to 6.5% of the total baseline drag

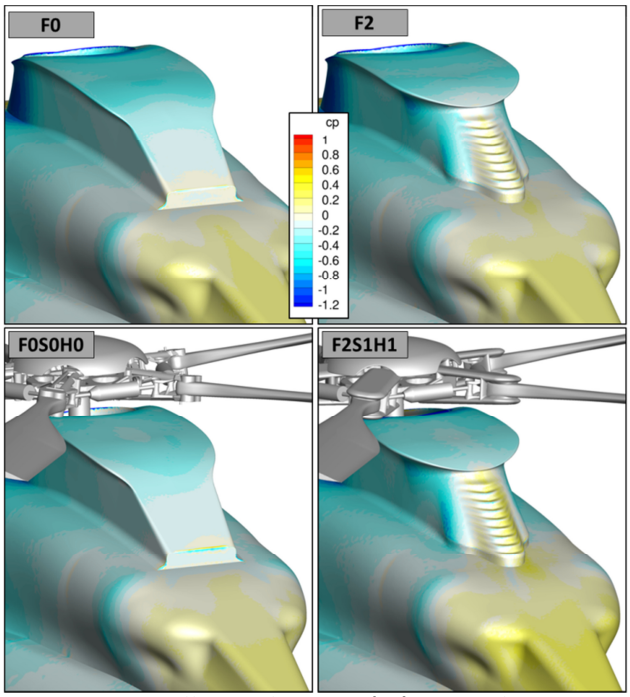

Figure 27 – Coefficient of pressure (Cp) at pylon fairing and cowlings; angle of attack of 0°

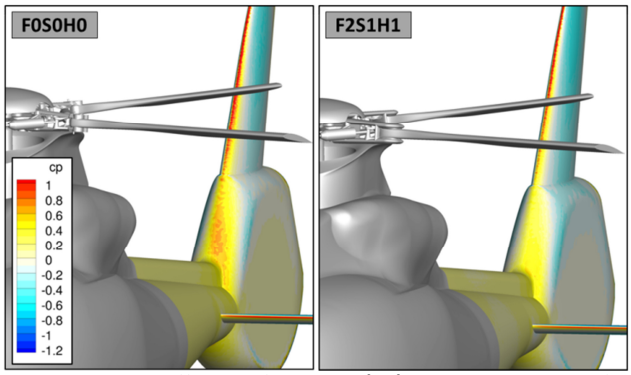

Figure 28 – Coefficient of pressure (Cp) at tail parts; angle of attack of 0°

at 0° of angle of attack is experienced for all the other tested angles of attack.

6. CONCLUSIONS

This paper deals with the assessment of the drag benefits obtained from the innovative hub fairings proposed with the framework of the Clean Sky GRC ITD CARD Partner Project.

The CARD Project consists in the experimental investigations of the capabilities of drag reduction from the use of two different innovative designs of pylon fairings together with two enhanced sleeve fairings and two advanced hub-cap designs. The Wind-Tunnel Tests (WTT) were performed at low-speed wind tunnel at VZLÚ in Prague (Czech Republic) on a 1:4 scaled Airbus Helicopters H155

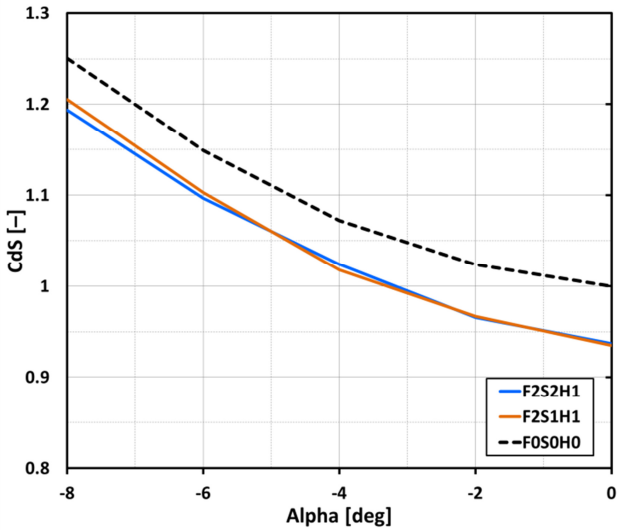

Figure 29 – Drag polar with respect to the angle of attack, for the best combination of fairings; Drag surfaces are normalized by the total model drag of the baseline configuration; sideslip angle of 0°

fuselage model with truncated rear parts. The model was mounted by a simplified 5-bladed rotor head.

Drag measurements for typical cruise flight conditions demonstrate benefits on drag of up to 6.5% of the baseline model drag for best combinations of fairings, without degrading the generation of lift. The best benefits on drag are obtained when partial sleeve fairings (S1) are used together with the smooth hub cap (H1). In this case, around 50% of the benefits come from a reduction of the rotor/fuselage interaction drag. Measurements also show that those benefits are very robust regarding the H/C angle of attack.

The different shapes investigated in the wind tunnel have also been studied numerically, at the same scale as for the experimental campaign, and for same flow conditions. Steady-state computations assuming a non-rotating rotor head have been achieved using the unstructured-mesh based DLR's TAU solver to assess by CFD the benefits on drag. The use of a fixed rotor head azimuthally located at 0° for all the computations has been motivated by the fact that drag polars were shown during the WTT campaign to be very similar to polars obtained with a rotating rotor, both in terms of dynamic drag and in terms of magnitude.

The simulations point out that for the baseline configuration (F0S0H0), airframe/flow interactions are responsible for 11% of the model total drag. They also demonstrate satisfying agreement with measurements, especially in terms of trends and ranking of configurations, despite an underestimation of up to 10% of the model drag surface. In particular the best benefits are obtained for the same combination as experienced during the WTT campaign, namely F0S1H1. For this configuration, the analysis shows that the benefits reach 9.7% of the baseline model drag assessed numerically. The benefits principally come from a reduction of the interactional drag for 45%, the rest being a reduction of parasite drag (for 55%). Those contributions to drag reduction are fairly similar to what measured during the WTT campaign. The most complex combinations involving innovative pylon fairing F2 (not investigated during WTT) in conjunction with the best rotor-head fairing S1H1 reveal potential benefits on drag of 11.6%.

The robustness of the benefits on drag obtained for the best combinations of fairings is observed numerically with respect to variations of angles of attack or sideslip angles.

In addition, numerical investigations have been carried out to assess the efficiency of the best combinations of innovative fairings on a complete H/C. This includes the potential interactions with the tail parts, together with more realistic baseline sleeves and additional rotor-head subcomponents, such as the lead-lag dampers. The analysis shows that the benefits on drag, reaching around 6.5% of the total drag, are well preserved for the best combination (F2S1H1), in spite of the presence of lead-lag dampers. The analysis shows that almost all the benefits come from a reduction of the interactions at the pylon fairings, at the aft cowlings as well as the shroud. The full sleeve fairings S2 are also a good candidate, as it offers a smooth aerodynamic integration of the lead-lag dampers.

ACKNOWLEDGEMENTS

The authors wish to thank the European Clean Sky JTI Green RotorCraft Programme for supporting the research activities presented in this paper under GRC ITD Grant Agreement Number CSJU-GAM-GRC-2008-001 and Grant Agreement Number 267571.

The authors are also grateful for the support from the CARD Consortium members, particularly R. Green & M. Giuni from University of Glasglow, and D. Zacho & J. Červinka from VZLÚ.

COPYRIGHT STATEMENTS

ABBREVIATIONS

CARD	Contribution to Analysis of Rotor-hub Drag reduction
CFD	Computational Fluid Dynamics
F*x*S*y*H*z*	Combination of fairings composed of pylon fairing #*x*, Sleeve fairing #*y* and hub cap #*z*
GRC	Green RotorCraft
JTI	Joint Technology Initiative
ITD	Integrated Technology Demonstrator

WTT Wind-Tunnel Tests

SYMBOLS

CdS	Drag surface	[m^2]
ClS	Lift surface	[m^2]
Cp	Coefficient of pressure	[–]
$\Delta q(\%)$	Dynamic pressure deficit (when < 0)	[–]
q	Dynamic pressure	[Pa]
ρ	Air density	[$kg \cdot m^{-3}$]
$\boldsymbol{U}$	velocity vector of air particle	[$m \cdot s^{-1}$]

REFERENCES

[1] Alfano, D. “Rotorcraft top fairing having a profile in the shape of a truncated drop of water that is provided with a hump of uneven surface”, Patent US2015147177, 2015.

[2] Alfano, D., Desvigne, D. & Fukari, R. “Rotor dome, a rotor & a rotorcraft”, Patent US2016137297, 2016.

[3] Desvigne, D. & Alfano, D. “Rotor-head/fuselage interactional effects on helicopter drag: influence of the complexification of the rotor-head geometry”, 39th European Rotorcraft Forum Proceedings, Moscow (Russia), 2013.

[4] Green, R.B., Giuni, M., Červinka, J., Zacho, D., Austin, P., Smith, S., Desvigne, D. & Alfano, D. “The Clean Sky CARD Project: Wind-tunnel measurements of a model helicopter rotor and fuselage drag”, 41st European Rotorcraft Forum, Munich (Germany), 2015.

[5] Jeong J. & Hussain F., “On the identification of a Vortex”, Journal of Fluid Mechanics, Vol 285, pp. 69-94, 1995.

[6] Johnson, W. “Helicopter theory”, Dover Publications, New York (USA), 1980.

[7] Johnson, W. “Rotorcraft aeromechanics”, Cambridge University Press, 2013.

[8] Leishman, J.G. “Principles of Helicopter Aerodynamics”, 2nd edition, Cambridge Aerospace Series, 2006.

[9] Logan, A.H., Marthe, R., Clark, D.R. & Phelps, A. “An Integrated Analytical and Experimental Investigation of Helicopter Hub Drag”, 35th American Helicopter Society Annual Forum Proceedings, Washington D.C. (USA), 1979.

[10] Roesch, P. & Dequin, A.M., “Experimental research on helicopter fuselage and rotor-hub wake turbulence”, 39th American Helicopters Society Annual Forum Proceedings, St Louis (USA), 1983.

[11] Roesch, P. & Vuillet, A. “New Designs for Improved Aerodynamic Stability on Recent Aerospatiale Helicopters”, 37th American Helicopter Society Annual Forum Proceedings, New Orleans (USA), 1981.

[12] Sheehy, T.W., “A method for predicting helicopter hub drag”, NTIS AD-A021 201, 1976.

[13] Stroub, R.H. & Rabbott, J.P. Jr. “Wasted Fuel – Another Reason for Drag Reduction”, 31st Annual National Forum of the American Helicopter Society, Washington D.C. (USA), 1975.

[14] Wagner, S.N. “Problems of Estimating the Drag of a Helicopter”, AGARD Conference Proceedings No. 124, Brussels (Belgium), 1973.

[15] Wilson, F.T., Fuselage Aerodynamic Design Issues & Rotor/Fuselage Interactional Aerodynamics. Part I Practical Design Issues, AGARD-R-781, 1990.

[16] http://www.cleansky.eu/

[17] http://tau.dlr.de/code-description/